J Nanopart Res (2017) 19: 282
DOI 10.1007/s11051-017-3971-y

RESEARCH PAPER

Oral intake of zirconia nanoparticle alters neuronal development and behaviour of *Drosophila melanogaster*

Monalisa Mishra · Debabrat Sabat · Basanti Ekka · Swetapadma Sahu · Unnikannan P · Priyabrat Dash

Received: 3 April 2017 / Accepted: 13 July 2017 / Published online: 8 August 2017

Abstract Zirconia nanoparticles (ZrO_2 NPs) have been extensively used in teeth and bone implants and thus get a chance to interact with the physiological system. The current study investigated the oral administration of various concentrations of ZrO_2 NPs synthesized by the hydrothermal method (0.25 to 5.0 mg L^{-1}) on *Drosophila* physiology and behaviour. The size of the currently studied nanoparticle varies from 10 to 12 nm. ZrO_2 NPs accumulated within the gut in a concentration-dependent manner and generate reactive oxygen species (ROS) only at 2.5 and 5.0 mg L^{-1} concentrations. ROS was detected by nitroblue tetrazolium (NBT) assay and 2′,7′-dichlorofluorescein (H2DCF) staining. The ROS toxicity alters the larval gut structure as revealed by DAPI staining. The NP stress of larvae affects the *Drosophila* development by distressing pupa count and varying the phenotypic changes in sensory organs (eye, thorax bristle, wings). Besides phenotypic changes, flawed climbing behaviour against gravity was seen in ZrO_2 NP-treated flies. All together, for the first time, we have reported that a ROS-mediated ZrO_2 NP toxicity alters neuronal development and functioning using *Drosophila* as a model organism.

Keywords Zirconia nanoparticles · *Drosophila melanogaster* · Toxicity · Behaviour · Sensory organs · Neurotechnology · Nanomedicine

M. Mishra (✉) · D. Sabat · S. Sahu
Neural Developmental Biology Laboratory, Department of Life Science, National Institute of Technology, Rourkela, Odisha 769008, India
e-mail: mishramo@nitrkl.ac.in

B. Ekka · P. Dash
Department of Chemistry, National Institute of Technology, Rourkela, Odisha 769008, India

U. P
School of Biology, IISER Thiruvananthapuram, Trivandrum, Kerala 695016, India

Introduction

Zirconia (ZrO_2) is widely used in the biomedical industry because of its inertness. Recently, zirconia nanoparticles (ZrO_2 NPs) are used in labelling, targeting, and drug loading (Nagy et al. 2016). Mesoporous zirconia has a greater surface area and thus is used for loading and targeted release of drug to cancer cells (Tang et al. 2010). Fluorescent-labelled zirconia is used for drug adsorption studies (Nagy et al. 2015). The functionalized ZrO_2 NPs (pagination, targeting, or labelling) are biocompatible and thus used for the treatment of oral, colon, or hepatocellular carcinoma (Al-Fahdawi et al. 2015; Sponchia et al. 2015). Amalgamation of ZrO_2 NPs like silica-zirconia-malic acid composite is used as a nanocarrier to deliver medicine into targeted tumour site (Nagy et al. 2016). Besides drug delivery, zirconia nanocomposites are used in implants due to their least side effects (Sotoudeh et al. 2013). ZrO_2 NPs provide high flexure strength with minimal ion release paralleled to other metallic implants (Kosmač et al. 1999; Lacefield 1999; Manicone et al. 2007). Zirconia has its

application in ball heads for making total hip replacements like femoral heads, dental fillings, and dental implants (Piconi and Maccauro 1999).

Besides their wide application, the small size of NPs allows them to penetrate inside the cell and interact with cell cytoplasm and nucleus, resulting in mutation (Albanese et al. 2012). Nanoparticle increases the ROS leading to cell damage in a size- or a concentration-dependent manner (Long et al. 2006; Karlsson et al. 2008; Wason et al. 2013). Alumina NPs can disturb the cell viability, distress mitochondrial function, and generate oxidative stress (Di Virgilio et al. 2010). Copper oxide NPs cause toxic effects on the liver and kidney on the experimental animal (Karlsson et al. 2008). Silver NPs generate ROS and lactate dehydrogenase leakage, leading to cell damage (Hussain et al. 2005). These studies give us the extent of damage that NPs can cause to living beings (Lewinski et al. 2008).

Since ZrO_2 is widely used in implants or as nanocarriers for drugs, it is highly essential to study its toxic effects (Clarke et al. 2003; Depprich et al. 2008). ZrO_2 NPs tested on Wistar rat reveal that these nanoparticles can increase the ROS production in the cell (Arefian et al. 2015). Since the toxicity of ZrO_2 NPs is less explored, it would be of great importance to check the toxic effects of ZrO_2 NPs using a model organism, *Drosophila melanogaster*. *Drosophila* share 75% genomic similarity with diseased human genomes (Fortini et al. 2000). Their short life span, easy handling, and fully sequenced genome allow us to use it as a model organism to check the toxicity of ZrO_2 NPs. The current study reconnoitres the toxic effect of ZrO_2 NPs on *Drosophila* sensory organ development and behaviour not described in earlier studies.

Materials and methods

Materials

Zirconyl chloride, sodium hydroxide, and sodium chloride were purchased from Sigma-Aldrich. Hydrogen peroxide, 2′,7′-dichlorofluorescein, trypan blue, and nitroblue tetrazolium were purchased from HiMedia. All chemicals purchased were of analytical grade and are used in the experiment as supplied by the company without any further purification.

Synthesis of ZrO_2 NPs

Synthesis of the ZrO_2 NP procedure followed the hydrothermal method, where 16.11 g of $ZrOCl_2 \cdot 8H_2O$ was dissolved in 100 mL deionized water. After dissolution, 1 M of NaOH solution was added dropwise to maintain pH 10. The solution was stirred continuously for 24 h, and the white precipitate obtained was centrifuged for four to five times to separate NaCl from the solution. The end product was autoclaved for 6 h at 200 °C followed by freeze drying. The obtained product was then subjected to calcination for 5 h at 350 °C. The product was then ground by a mortar and pestle to get ZrO_2 NPs (Liang et al. 2002).

Characterization of nanoparticle

FT-IR analysis

The FT-IR spectroscopy (Perkin-Elmer) was used to determine the functional groups present in ZrO_2 NPs. The spectrum was scanned from 4000 to 400 cm^{-1}. Nearly 3–4-mg sample was mixed with 30 mg of KBr and the pallet was formed. The pellet was stored in a vacuum desiccator and IR lamp exposed for 1 min before the analysis.

XRD analysis

The powdered sample was subjected to X-ray diffractometer (XRD) analysis to check the phase of ZrO_2 NPs. The phase of the synthesized nanoparticle was determined by an X-ray diffractometer (Rigaku Japan/Ultima-IV) with CuK_α radiation (λ = 0.154 nm), 2θ range 10°–80°, and scan rate 2° per minute.

Field emission scanning electron microscopy and transmission electron microscopy

The size, structure, and morphology of the nanoparticles were investigated by using field emission scanning electron microscopy (Nova NanoSEM/FEI). The sample was prepared by dispersing ZrO_2 NPs. Then, one drop of the suspension was spread over ITO glass slides for analysis. ZrO_2 NPs were spread over carbon-coated copper grids. The transmission electron micrographs (PHILIPS CM 200), HRTEM, and SAED pattern of the ZrO_2 NPs were also analysed.

Zeta potential

The ZrO_2 NPs were dispersed in Milli-Q water and sonicated for 20 min; then, the zeta potential was measured using Malvern NANO-ZS-90.

Fly rearing and treatment

The *Oregon-R* (*OR*) flies were obtained from the Fly Facility, C-CAMP, Bengaluru, India. The standard fly food was prepared from sucrose, yeast powder, corn meal, and agar agar type I. ZrO_2 NPs of appropriate concentrations were added to the food in the treatment vial. Five different concentrations (0.25, 0.5, 1.0, 2.5, and 5.0 mg L^{-1}) were chosen for this study, including control (untreated). All the flies were kept in 25 °C and 12-h light and dark condition.

Life cycle

The life cycle of the *Drosophila* egg to adult development was compared to check for any developmental delay. The life cycle was checked every 6-h time interval for the developmental stages of *Drosophila* (i.e. egg, first-instar-third-instar larvae, pupa, and adult). The percentage of pupa formed and the adult hatched can be clearly noted to understand more about the delay or damage.

SEM and EDS for analysis of zirconia in larval midgut

The larval guts were dissected from the treated larvae and stored in 4% paraformaldehyde (PFA). Sample preparation for the SEM analysis was done by washing the gut with phosphate-buffered saline (PBS) and dehydrating it with a graded series of ethanol (30–100%). Before the dehydration step, a puncture was made using a needle in the midgut region; the opening will help us to measure the zirconia content within the gut.

Trypan blue exclusion test

The trypan blue staining distinguishes the dead from the live cells and can be used to check the damage in the gut by following the reported protocol with slight modification (Krebs and Feder 1997). The third-instar larvae were treated with 0.02% of trypan blue solution for 30 min, and then, the larvae were washed with 1× PBS for 15–20 min to wash off excess stain. The larvae were then imaged for staining from all the concentrations (Siddique 2012).

Larva crawling behaviour

The crawling behaviour of the third-instar larvae was checked by allowing the larvae to crawl over solidified 2% agarose gel prepared in a 90-mm petri dish. The crawling was recorded, and the speed was calculated (Nichols et al. 2012).

NBT reduction assay for ROS detection

To check the reactive oxygen species formed in the larva haemolymph with exposure to different concentrations of ZrO_2 NPs, the nitroblue tetrazolium reduction test was done. The haemolymph was extracted from 30 third-instar larvae. Nitroblue tetrazolium was added to it and left for 1 h in incubation at 30 °C in the dark. The reaction was stopped by the addition of one volume of acetic acid to it. The mixture was centrifuged at 12,000 rpm for 1 min. One hundred fifty microliters of 50% acetic acid was added to the pellet and vortexed vigorously for 5 min. Absorbance was taken at 595 nm using a PerkinElmer 2030 plate reader (Sabat et al. 2016).

DAPI and H2DCF larval midgut staining

Third-instar larvae gut was dissected and kept in 4% paraformaldehyde (PFA) at 4 °C. For staining, the PFA was removed from all the samples and 1 mL of PBS was added three times to rinse the PFA. After 10 min, the PBS was replaced by phosphate-buffered saline with Tween 20 (PBST). The samples were rinsed with PBST for three times, 10 min each wash. After the PBST wash, 2′,7′-dichlorofluorescein dye was added to the samples in the dark and incubated for 30 min. Later, the gut was rinsed with PBS in order to remove the extra dye and finally mount with DAPI and 20% glycerol mountant. The gut imaging was done using a fluorescence (Olympus IX71) microscope (Ohlstein and Spradling 2006; Gupta et al. 2007).

Adult weight

For weight measurement of the adult, 50 flies (25 males and 25 females) were collected from each experimental vial. The fly weight was measured by a fine weighing balance from all the treated vials. The average weight of each treatment vial was calculated and plotted in the graph.

Adult climbing behaviour

Thirty adult flies were isolated from each experimental vial and transferred into a 100 mL measuring cylinder in order to perform the climbing assay. The mouth of the cylinder was closed by a cotton plug. The cylinder was marked at 10 cm. Then, the cylinder was tapped two to three times so that all the flies come down to the bottom. Then, the flies were allowed to climb upwards for 15–20 s. The number of the flies which climbed up above the 10 cm mark within 10 s was recorded (Martinez et al. 2007).

Survivorship assay by H_2O_2 treatment

To check the stress resistance of the flies, H_2O_2 assay was performed. Twenty adult flies were taken from each treated vial and kept in an empty vial, carrying a Whatman paper soaked in 5% sucrose and 9% H_2O_2. The treated flies were compared against the positive and negative controls, and the number of flies dying was noted in an hourly interval (Posgai et al. 2011).

Adult phenotype

For phenotype analysis, 50 individual flies from each vial were observed under a stereomicroscope. Major abnormalities were observed in the eye, bristles, wings, and abdomen.

Statistical analysis

The data were analysed by using the GraphPad Prism 6.0 software. The data are represented as mean ± standard error, and statistical analysis was performed using unpaired Student's t test with $P < 0.05$ considered as the level of significance.

Results

Nanoparticle characterization

FT-IR analysis

The FT-IR spectra for the synthesized ZrO_2 NPs detect the presence of functional groups (Fig. 1a). The strong band at 3422 cm^{-1} corresponds to the stretching vibration of the –OH bond. Two bands at 1625 and 1362 cm^{-1} correspond to the bending vibration of the –OH bond due to water molecules absorbed on the surface of ZrO_2 NPs. A sharp peak at 725 and 557 cm^{-1} attributed to Zr–O stretching vibrations. The FT-IR data are reliable with the mesoporous ZrO_2 NPs.

XRD analysis

The XRD patterns of mesoporous ZrO_2 NPs were observed in Fig. 1b. Four broad peaks at 30.25°, 34.08°, 50.39°, and 59.81° are characteristic of the presence of the tetragonal phase of ZrO_2 (t-ZrO_2). Other types of ZrO_2, e.g. the monoclinic and cubic phases of zirconia, were also detected.

Field emission scanning electron microscopy (FESEM) and transmission electron microscopy (TEM)

The surface morphology of the synthesized nanoparticle was analysed by FESEM (Fig. 1c). The FESEM image illustrates the spherical particles of ZrO_2 with high aggregation, which leads to high surface area of the synthesized material (Fig. 1d). The particles are spherical in shape, and the size ranges from 10 to 12 nm (Fig. 1d'), as shown in size distribution curve.

The TEM image of ZrO_2 NPs divulges the multicrystal pore wall with lattice spaces of 0.31 and 0.28 nm and the interplanar distance (101) and (111), respectively (Fig. 1e). The corresponding selected area electron diffraction (SAED) pattern (Fig. 1e') of the spherical ZrO_2 NPs indicates the high nanocrystalline nature of the synthesized material, which can be indexed to the (101) and (111) planes. The d-spacing corresponding to the diffraction rings of the SAED pattern was in agreement with the tetragonal phases of mesoporous ZrO_2 NPs.

Zeta potential

The ZrO_2 NPs suspended in the Milli-Q water were subjected to sonication for more than 20 min, and then, the zeta potential was measured (Fig. 1f). The zeta potential of ZrO_2 NPs was found to be −14.9 mV, which explains the agglomeration as observed in FESEM and TEM images (Fig. 1c, d).

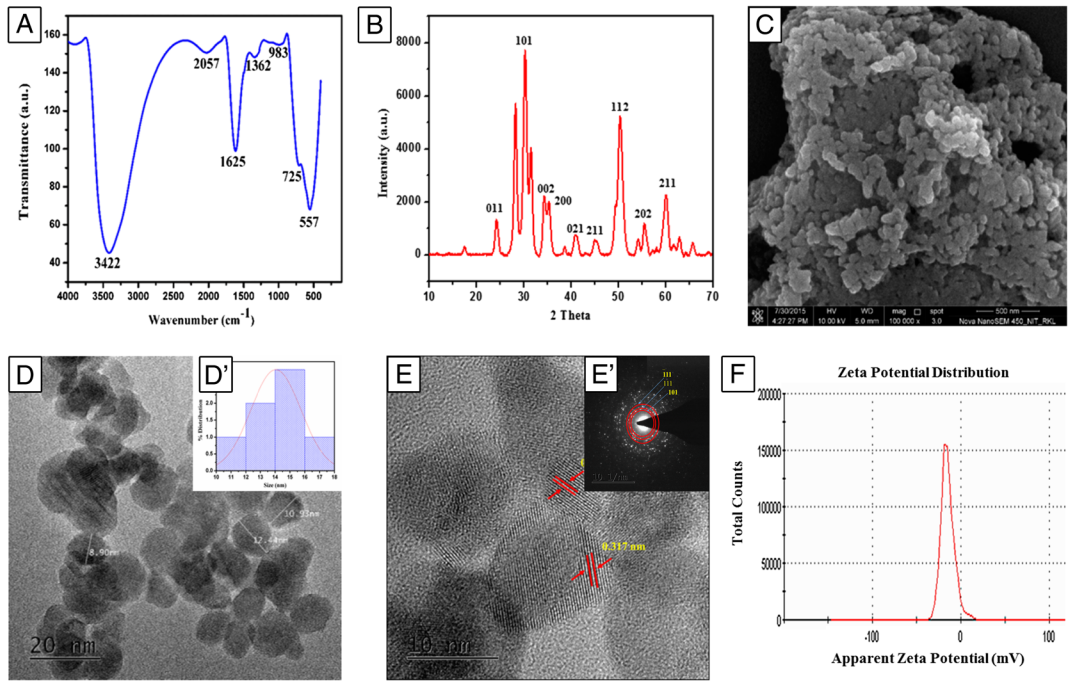

Fig. 1 Characterization of zirconia NPs. **a** FT-IR pattern of zirconia nanoparticle. **b** XRD pattern of zirconia. **c** FESEM image of ZrO_2 NPs. **d** TEM image of ZrO_2 NPs. **d'** Histogram of size distribution of ZrO_2 NPs. **e** HRTEM image showing $d = 0.315$. **e'** SAED pattern of ZrO_2 NPs. **f** Zeta potential of ZrO_2 NPs

SEM-EDS of the midgut

The SEM-EDS of the midgut was taken from the pricked region in the dissected gut of *Drosophila*. The elemental analysis confirmed the presence of zirconia within the gut. The concentration of zirconia in the treated gut was more from control; with increasing concentration the treated larvae shows rising peaks of zirconia (Fig. 2a).

Life cycle

The abnormality in the stages of development from egg to adult elucidates the role of stress in developmental cycle. To understand the effect of ZrO_2 NPs, developmental stages after treatment were closely observed in every 6-h interval. At higher concentration, 2 days of developmental delay was observed (Fig. 2b).

Trypan blue exclusion test

Trypan blue dye differentiates dead cells against live cells in the tissue. Trypan blue-stained guts from different treatments were imaged under a stereo microscope (Fig. 2c). No staining was observed in any of the treated larvae.

Larva crawling behaviour

The third-instar larvae are voracious feeders and thus have more chance to take NPs. The larvae move by making body contractions. These contractions create a wave to move or locate themselves to another point. These contractions were directly controlled by the motor neurons in the larval brain (Zhang et al. 2014). So, any abnormality in neuron reflects defective larvae crawling pattern. The speed and the tracking pattern of the path were plotted using the Ctrax software (Fig. 2d, e). The larva speed was unaltered, except in 0.5 mg L^{-1} vial where a more disturbed track pattern was observed. The number of turn's stops was more with increasing concentrations, which signifies that it might not be affecting the contraction but altering the neurons to walk straight and follow a confused pattern.

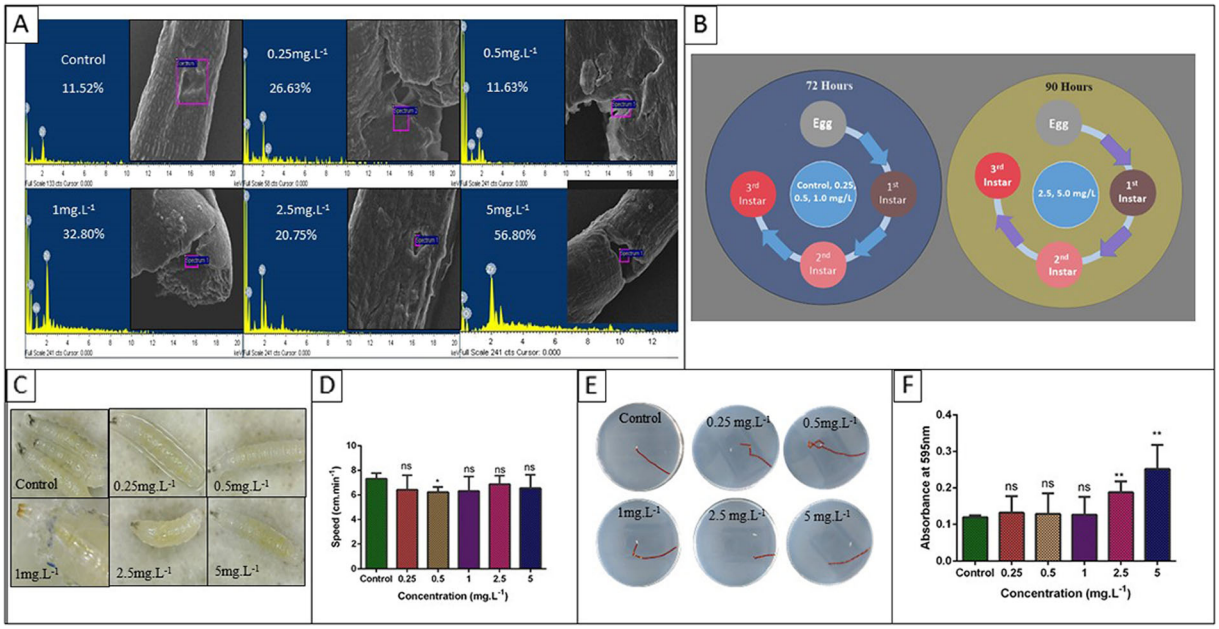

Fig. 2 ZrO_2 NP effect on various elemental, physiological, and behavioural parameters of the larvae. **a** SEM-EDS imaging for zirconia analysis. **b** Life cycle delay in larvae formation. **c** Trypan blue staining of the larva to check for gut damage. **d** Larva crawling speed. **e** Tracking pattern of the larva. **f** NBT reduction assay for the ROS estimation. The significant results are marked with *asterisks* (*ns* non-significant, * for *P* value <0.05, ** for *P* value <0.007)

NBT reduction assay for ROS detection

NBT assay was used to quantify the amount of free radicals generated within the body. To check the amount of free radicals generated by ZrO_2 NPs, the haemolymph from the third-instar larvae was collected. The free radical formation upsurges the ROS formation, which is mainly responsible for the oxidative damage. At 2.5 and 5.0 mg L^{-1} concentrations' increased absorbance for NBT reduction was observed (Fig. 2f).

DAPI and H2DCF staining

DAPI and 2′,7′-dichlorofluorescein (H2DCF) stain the nucleus and the ROS region of the gut, respectively. To check for the amount of reactive oxygen species generated due to oral intake of NPs, the fly gut (Fig. 3a) was dissected and stained with DAPI and H2DCF dye. The gut was analysed under a fluorescence microscope. DAPI staining shows the status of the nucleus. With increasing concentrations of ZrO_2 NPs, the aggregated nucleus was observed in the gut (Fig. 3b). Staining with H2DCF showed an increase in the intensity with concentration of ZrO_2 NP. A significant amount of increase in staining was observed in 2.5 and 5.0 mg L^{-1} (Fig. 3c) when compared with the control.

Percentage of pupae and flies hatched

The percentage of pupa formed in the ZrO_2 NP treatment vials found to decrease significantly. The decrease in 2.5 and 5.0 mg L^{-1} was significant and found to be 72.43 ± 8.18 and 68.78 ± 2.6%, respectively (Fig. 4a). Similarly, the flies hatched from the pupa found to decrease and were comparable with the percentage of pupa formation 75.66 ± 1.50 and 65.36 ± 2.10% for the concentrations 2.5 and 5.0 mg L^{-1} (Fig. 4b).

Adult weight

The weight of the 50 flies was taken and compared. Increasing concentrations of nanoparticle affect the metabolic activity of the body by altering the body weight (Fig. 4c). The body weight increases non-significantly in 0.25, 0.5, and 1.0 mg L^{-1} exposures. At 5 mg L^{-1}, the body weight decreases significantly ~11% with respect to the control.

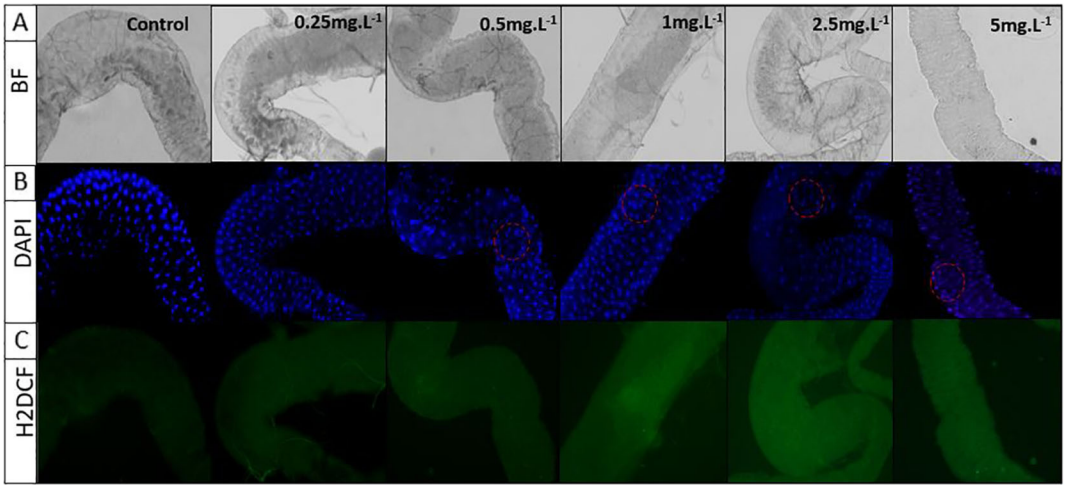

Fig. 3 Larva midgut imaging for nucleus staining and ROS detection. **a** Bright field (BF). **b** DAPI. **c** 2′,7′-Dichlorofluorescein (H2DCF) staining for ROS in the gut. DAPI staining revealed presence of micronuclei-like structures circled while the increasing green florescence with increasing zirconia treatment signified ROS generation

Adult climbing behaviour

Adult climbing behaviour helps to assay the functioning of the antenna, which is responsible for sensing the gravitational pull and help them to maintain a proper balance during flight (Bokolia and Mishra 2015). With exposure towards nanoparticles, impaired climbing behaviour was observed in a concentration-dependent

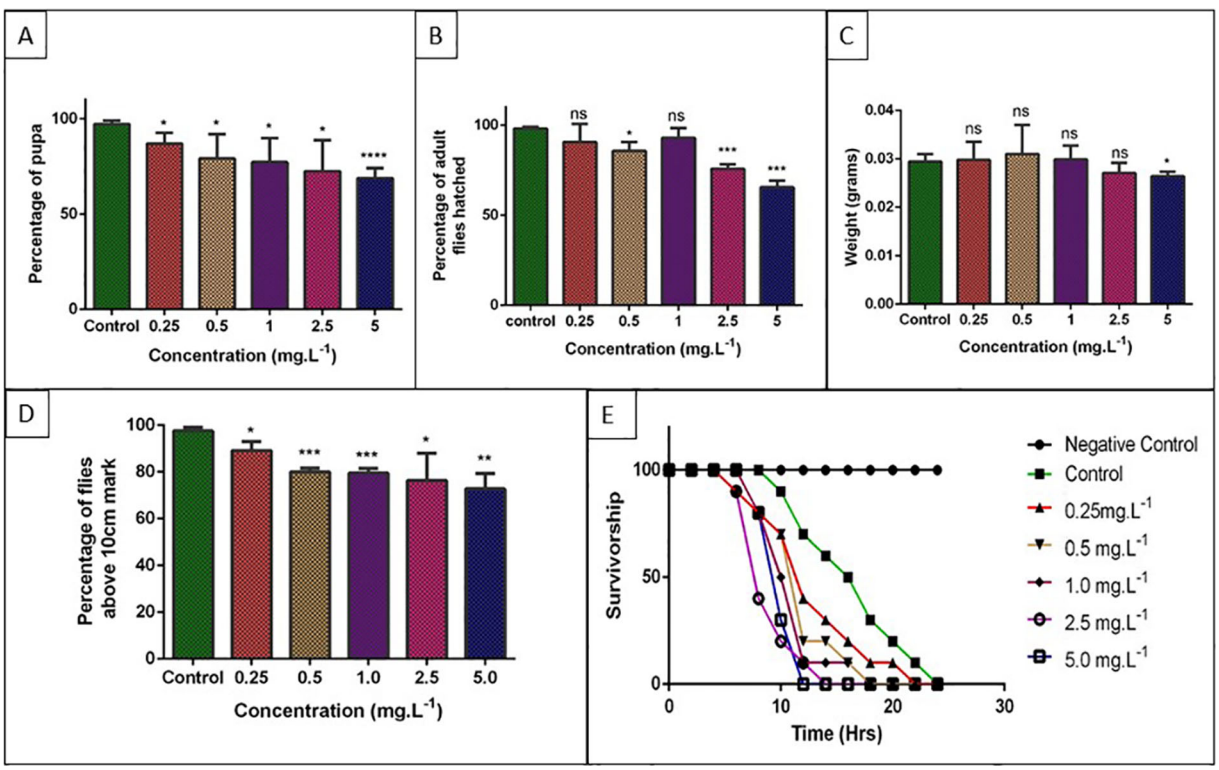

Fig. 4 Assessment of pupa count, adult hatching, weight, and behaviour. **a** Percentage of pupa formed. **b** Percentage of adult flies hatched. **c** Weight of flies. **d** Climbing assay: percentage of flies that can climb above 10-cm mark in 10 s. The results found significant to control are with *asterisks*. **e** H_2O_2 assay for checking the endurance of treated flies (* for *P* value <0.05, ** for *P* value <0.003, *** for *P* value <0.0002, **** for *P* value <0.00001)

manner. In 0.25 mg L^{-1}, 89.22 ± 2.22% flies can climb above the 10-cm mark. In 0.5 and 1.0 mg L^{-1}, the percentage of flies affected was 80.07 ± 0.92 and 79.51 ± 1.11%, respectively. The major difference was observed at higher concentration where 76.40 ± 6.7% of 0.25 mg L^{-1} and 72.77 ± 3.74% of 0.5 mg L^{-1} could only climb upwards (Fig. 4d).

Survivorship assay by H_2O_2 treatment

The survivorship assay helps to calculate the flies' capacity to tolerate stress, via the innate mechanism of antioxidant production. It is explained that the stressed flies can endure less stress than the control. The flies from 1.0 to 5.0 mg L^{-1} died earlier than the other treatments, while 2.5 mg L^{-1} flies were slightly comparable to control flies (Fig. 4e).

Adult phenotypes

The accumulated stress during development kindled from the NP stress changes the cell development and tissue differentiation resulting in abnormal phenotype in flies treated with ZrO_2 NPs. Abnormalities were found in the eye, thorax bristles, and wings as a result of toxicity of NPs.

Eye phenotype

The eye is formed by many ommatidia, which is affected due to nanoparticle exposure. The ommatidia units were observed to be fused, and rough eye phenotype was observed in 0.25, 1.0, and 5 mg L^{-1}. The ommatidia are misoriented in 0.5 mg L^{-1}, and blisters are observed in the 2.5 mg L^{-1} (Fig. 5a).

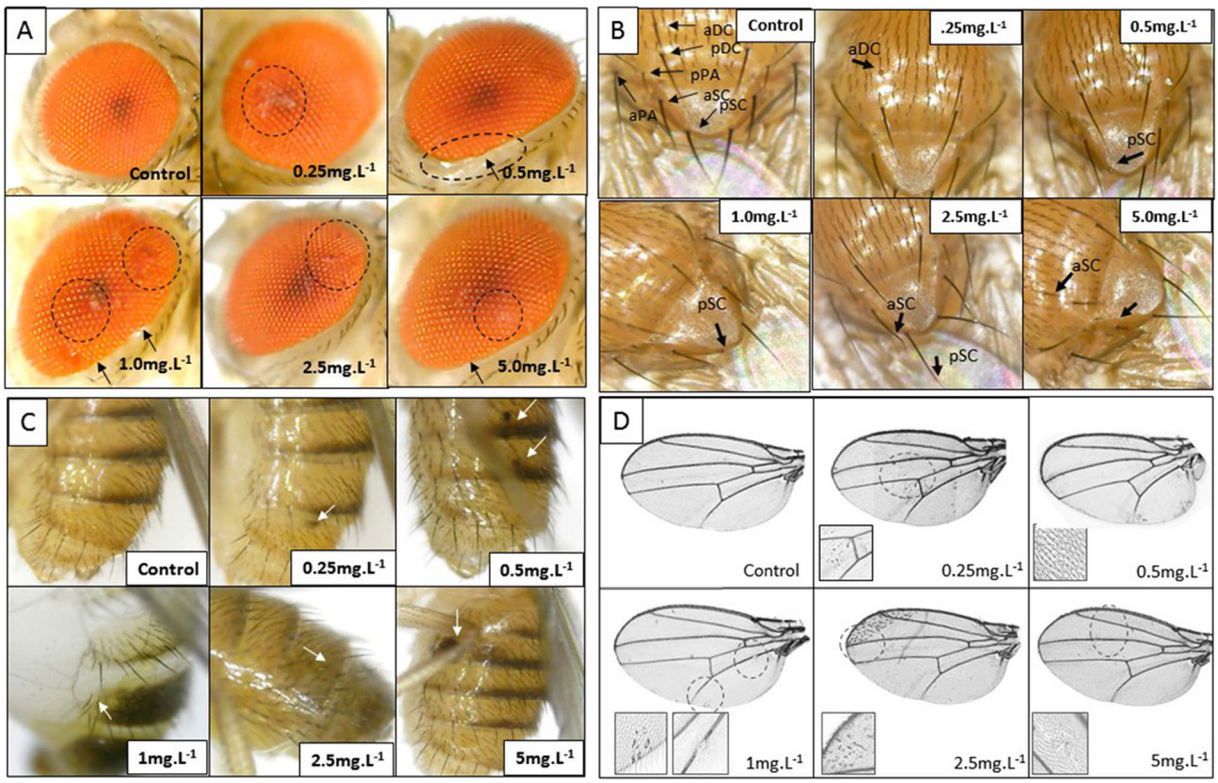

Fig. 5 Phenotype observation. **a** Eye: at 0.25 and 1.0 mg L^{-1} increasing concentrations, the ommatidia were observed to be affected as indicated in *circles*, while in at 0.5, 1.0, and 5.0 mg L^{-1} concentrations, there was marginal loss in ommatidia as indicated by *arrows*. **b** Thorax bristles: bristles were found to be lost in non-orderly fashion mostly from pSC, aDC, and aSC regions in almost all the concentrations, but at 2.5 mg L^{-1}, the bristles showed abnormal bent elongation. **c** Abdomen: dark spots similar to melanization are observed near the abdomen segments at 0.25, 0.5, and 5.0 mg L^{-1}, while at 1 mg L^{-1}, the abdomen was abnormally bulging, and at 2.5 mg L^{-1}, the segments appeared faint. **d** Wings: the trichomes were found to be affected in all the treated fly wings, which happened due to defective planar polarity; trichomes either appeared to be fused or were missing

Bristle phenotype

Bristles present on the thorax are part of the external sensory organs which were affected by exposure to nanoparticles. Out of 13 pairs of bristles (macrochetes), random loss was seen in NP-treated vials. In 0.25 mg L^{-1} treatment, the anterior dorsocentral (aDC) is absent; posterior scutellar (pSC) is affected in both 0.5 and 1.0 mg L^{-1}. Both aDC and anterior scutellar (aSC) bristle losses were observed in 5 mg L^{-1} (Fig. 5b). The occurrence of such loss in macrochaetes was found to be random when compared to the control.

Abdomen phenotype

The abdomen of the fly was found to be affected at a higher concentration of ZrO_2 NPs. Black spots were found at various locations in 0.25, 0.5, and 5.0 mg L^{-1} treated vials (Fig. 5c). In few concentrations, bulging abdomens were found (in the 1 mg L^{-1}). Segment decolouration was also observed in 2.5 and 5.0 mg L^{-1}.

Wing phenotype

Wing develops from wing imaginal disc, which is essential for flight and balancing of the body. The wing venation pattern was affected due to the treatment of ZrO_2 NPs. Similar to that of microchaetes in thorax, there are trichomes over the cuticle of the wing. The trichome arrangements are required for flight, sensation, and control. The nanoparticle exposure affects the trichome arrangement within the wing in all the concentrations ranging from 0.25 to 2.5 mg L^{-1}. Trichomes were missing in 5.0 mg L^{-1} (Fig. 5d).

Discussion

Zirconium (available in the form of zirconium oxide) is chemically inert and thus offers itself for wide biological use (Aboushelib et al. 2008). Besides its inertness, the current study reports the accumulation of ZrO_2 NPs within the gut in a concentration-dependent manner. How do ZrO_2 NPs accumulate within the gut? The ZrO_2 NPs has a negative surface charge (−14.1 mV) that allows the NPs to interact with gut proteins and hence help in the accumulation within the gut. Are the accumulated NPs toxic for the cell or the tissue? To explore the ZrO_2 NP toxicity within the gut, the third-instar larvae were stained with trypan blue which distinguishes between live and dead cells. A faint staining was marked in few larvae of 1 mg L^{-1} concentration in the hindgut, suggesting that ZrO_2 NPs do not cause much damage to the gut of third-instar larvae. The gut is lined by peritrophic membrane with pores (Lehane 1997) for exchange of materials. The NPs cross the peritrophic membrane, enter into the haemolymph, and produce free radicals. The amount of the free radicals was evidenced from the NBT assay done in third-instar larvae of 2.5 and 5.0 mg L^{-1} concentrations. DAPI staining reveals blebbed nuclei only at higher concentration. Earlier, zirconium ions >0.5 mM are known to induce an apoptotic effect in human (jurkat) T cells (Caicedo et al. 2008) and mouse cell line (Catelas et al. 1999). ZrO_2 NP treatment is further associated with faulty signal transduction, cell cycle regulation, immunity, and downregulation of vesicular transport genes (Carinci et al. 2004; Sollazzo et al. 2008). Neuronal cell lines (PC12 and N2a) when tested for the toxicity with ZrO_2 NPs showed cytotoxic and genotoxic effects in a dose- and time-dependent manner for concentration >31 mg L^{-1} (Asadpour et al. 2016). The toxicity found in those cell lines is due to an increase of ROS and malondialdehyde and a decrease of intracellular cell glutathione content (Asadpour et al. 2016). In the current study, we also observe an increase of ROS in 1.0–5.0 mg L^{-1} treated flies, which is evidenced by H2DCF staining and NBT assay.

Nevertheless, the larva crawling behaviour, which indicates the functionality of neuromuscular activity and dopaminergic neurons, was found to be affected, as concluded from decreased crawling speed on ZrO_2 NP treatment (Barone and Bohmann 2013). The rhythmic pattern of *Drosophila* locomotion is an action of multiple dendritic (MD) neurons. Thus, any damage or disruption of these MD neurons prolongs stereotype firing within posterior to anterior segment, resulting in arrhythmic larva crawling in the treatment vial (Song et al. 2007).

Drosophila undergoes metamorphosis from pupa to adult immediately after crossing the third-instar larval stage (Takashima and Hartenstein 2012). During this stage, several modifications in the body occur, where the entire gut gets replaced with new cells (Takashima and Hartenstein 2012). During these transitions, the ZrO_2 NPs get an opportunity to interfere with the whole-body mechanism, which accounts for a decrease

in the pupae count. ZrO_2 NPs are known to interact with proteins and may affect the normal expression and development (Lima et al. 2008; Lynch and Dawson 2008). In the current study, a number of flies hatched from pupae were found to be decreased. ZrO_2 NPs did not alter the fly weight even at an exposure of higher concentration. The climbing behaviour signifies the ability to move against gravity and neuronal homeostasis (Barone and Bohmann 2013; Bokolia and Mishra 2015). Control flies are able to sense gravity and balance the body, while in ZrO_2 NP-exposed flies, there is a decreased climbing ability around ~25% after 5 mg L^{-1} ZrO_2 NP exposure. Similar results were also observed when flies were exposed to TiO_2 NPs at higher concentrations (200 and 250 mg L^{-1}) (Sabat et al. 2016). Analogous reports of defective antennae were also observed after alumina NP (Huang et al. 2013) and hydroxyapatite NP (Pappus et al. 2017) exposure.

The phenotypic defects observed in ZrO_2 NP-treated flies include an abnormality in the eye, thorax bristles, abdomen, and wing trichomal hairs. The different eye phenotypes observed were rough eye and misoriented and fused ommatidia. Fused ommatidia are associated with bristle loss or developmental defect in the eye due to endosomal glycoprotein dimer secretion and via regulation of notch and delta activity (Li et al. 2003; Artavanis Tsakonas et al. 1999; Brand and Perrimon 1993). In order to maintain the geometrical hexagonal array for the ommatidia, around 1500–2000 cells have to be eliminated from the retinal epithelium (Wolff and Ready 1991). Any defect in the elimination process resulted in surplus cells and rough eye (Wolff and Ready 1991). Near to the margin of the eye, irregular ommatidial arrangements were observed in 0.5 and 1.0 mg L^{-1}. The eye phenotype further explains the notch or delta pathway embarrassment during development.

The thorax bristle macrochaetes were affected during development after nanoparticle exposure, as observed in TiO_2 NP treatment (Sabat et al. 2016). Several signalling and patterning factors are responsible for 13 pairs of macrochaete orientation on *Drosophila* thorax (Held 1991). The bristle morphogenesis is a three-stage process, starting with the successive division of single-organ precursor cells (Claxton 1969). The proneural gene achaete-scute (AS-C) and signalling pathways of notch and EGFR intracellular regulation cause the morphogenesis of these pro-neural cluster cells that is involved in bristle formation (Culí et al. 2001). Missing aDC bristles are found in $wg^{Sp\text{-}1}$/wg^{CX4} mutants in which the expression of *wg* on notum is strongly reduced and restricted to posterior notum (Yang et al. 2012). Long bent phenotype is observed in few bristles of aSC and pSC in 2.5 mg L^{-1}. A comparable phenotype is known to occur in "singed mutants" with defects in the composition and organization of actin filaments. Zirconia composite is known to increase beta-actin expression (Cant et al. 1994; Ko et al. 2007). The bristle phenotype suggests that with increasing concentrations of ZrO_2 NPs, beta-actin amount increases and it alters the bristle phenotype in the current study.

The abdomen spots were observed in 0.25, 0.5, and 5.0 mg L^{-1} (marked with a white arrow) near the abdominal segment. Abdomen spots were reported due to melanization or pigmentation. Mechanically, such spots are due to defective copper homeostasis (Armstrong et al. 2013). Abdomen bulging in a few more instances was found in 1 mg L^{-1} treated vial, although such occurrence was rare in lower concentration. All these phenotypes suggest that ZrO_2 NPs affect the haemolymph, cause melanization, and impair abdomen development. Defective trichome arrangements were observed in the wing of almost all the treated concentrations. The planar polarity of the gene *multiple wing hairs* (*mwh*) is responsible for such phenotype (Goodrich and Strutt 2011). Any alteration in the expression of *mwh* might have been affected during development, resulting in such a wing phenotype. Altered wing phenotype suggests that the expression of *mwh* was altered due to nanoparticle treatment. How nanoparticle-mediated ROS affect the gene regulation/expression and alter the phenotype needs to be explored in a developmental time window to understand the mode of action of ZrO_2 NPs.

Acknowledgments We are thankful to S. Aurosman Pappus for his help in larva video tracking. We are thankful to Prof. Santanu Paria laboratory for zeta potential analysis of the sample and technical staff of NIT Rourkela for handling SEM and TEM facility.

Compliance with ethical standards

Funding P. Unnikanan is thankful to DST-Inspire Fellowship for financial support.

Conflict of interest The authors declare that they have no conflict of interest.

References

Aboushelib MN, Matinlinna JP, Salameh Z, Ounsi H (2008) Innovations in bonding to zirconia-based materials: part I. Dent Mater 24:1268–1272

Albanese A, Tang PS, Chan WC (2012) The effect of nanoparticle size, shape, and surface chemistry on biological systems. Annu Rev Biomed Eng 14:1–16

Al-Fahdawi MQ, Rasedee A, Al-Qubaisi MS, Alhassan FH, Rosli R, El Zowalaty ME, Naadja SE, Webster TJ, Taufiq-Yap YH (2015) Cytotoxicity and physicochemical characterization of iron–manganese-doped sulfated zirconia nanoparticles. Int J Nanomedicine 10:5739–5750

Arefian Z, Pishbin F, Negahdary M, Ajdary M (2015) Potential toxic effects of zirconia oxide nanoparticles on liver and kidney factors. Biomed Res 26:89–97

Armstrong N, Ramamoorthy M, Lyon D, Jones K, Duttaroy A (2013) Mechanism of silver nanoparticles action on insect pigmentation reveals intervention of copper homeostasis. PLoS One 8:e53186

Asadpour E, Sadeghnia HR, Ghorbani A, Sedaghat M, Boroushaki MT (2016) Oxidative stress-mediated cytotoxicity of zirconia nanoparticles on PC12 and N2a cells. J Nanopart Res 18:1–13

Barone MC, Bohmann D (2013) Assessing neurodegenerative phenotypes in *Drosophila* dopaminergic neurons by climbing assays and whole brain immunostaining. JoVE (J Vis Exp) e50339

Bokolia NP, Mishra M (2015) Hearing molecules, mechanism and transportation: modeled in Drosophila melanogaster. Dev Neurobiol 75:109–130

Brand AH, Perrimon N (1993) Targeted gene expression as a means of altering cell fates and generating dominant phenotypes. Development 118:401–415

Caicedo M, Jacobs JJ, Reddy A, Hallab NJ (2008) Analysis of metal ion-induced DNA damage, apoptosis, and necrosis in human (Jurkat) T-cells demonstrates Ni^{2+} and V^{3+} are more toxic than other metals: Al^{3+}, Be^{2+}, Co^{2+}, Cr^{3+}, Cu^{2+}, Fe^{3+}, Mo^{5+}, Nb^{5+}, Zr^{2+}. J Biomed Mater Res A 86:905–913

Cant K, Knowles BA, Mooseker MS, Cooley L (1994) *Drosophila* singed, a fascin homolog, is required for actin bundle formation during oogenesis and bristle extension. J Cell Biol 125: 369–380

Carinci F, Pezzetti F, Volinia S, Francioso F, Arcelli D, Farina E, Piattelli A (2004) Zirconium oxide: analysis of MG63 osteoblast-like cell response by means of a microarray technology. Biomaterials 25:215–228

Catelas I, Petit A, Zukor DJ, Marchand R, Yahia LH, Huk OL (1999) Induction of macrophage apoptosis by ceramic and polyethylene particles in vitro. Biomaterials 20:625–630

Clarke I, Manaka M, Green D, Williams P, Pezzotti G, Kim Y, Ries M, Sugano N, Sedel L, Delauney C (2003) Current status of zirconia used in total hip implants. J Bone Joint Surg 85:73–84

Claxton J (1969) Mosaic analysis of bristle displacement in *Drosophila*. Genetics 63:883–896

Culí J, Martín-Blanco E, Modolell J (2001) The EGF receptor and N signalling pathways act antagonistically in Drosophila mesothorax bristle patterning. Development 128:299–308

Depprich R, Zipprich H, Ommerborn M, Naujoks C, Wiesmann HP, Kiattavorncharoen S, Lauer HC, Meyer U, Kübler NR, Handschel J (2008) Osseointegration of zirconia implants compared with titanium: an in vivo study. Head Face Med 4:1–8

Di Virgilio A, Reigosa M, Arnal P, De Mele MFL (2010) Comparative study of the cytotoxic and genotoxic effects of titanium oxide and aluminium oxide nanoparticles in Chinese hamster ovary (CHO-K1) cells. J Hazard Mater 177:711–718

Fortini ME, Skupski MP, Boguski MS, Hariharan IK (2000) A survey of human disease gene counterparts in the Drosophila genome. J Cell Biol 150:23–30

Goodrich LV, Strutt D (2011) Principles of planar polarity in animal development. Development 138:1877–1892

Gupta SC, Siddique HR, Mathur N, Vishwakarma AL, Mishra RK, Saxena DK, Chowdhuri DK (2007) Induction of hsp70, alterations in oxidative stress markers and apoptosis against dichlorvos exposure in transgenic *Drosophila melanogaster*: modulation by reactive oxygen species. Biochim Biophys Acta 1770:1382–1394

Held LI (1991) Bristle patterning in *Drosophila*. BioEssays 13: 633–640

Huang N, Yan Y, Xu Y, Jin Y, Lei J, Zou X, Ran D, Zhang H, Luan S, Gu H (2013) Alumina nanoparticles alter rhythmic activities of local interneurons in the antennal lobe of *Drosophila*. Nanotoxicology 7:212–220

Hussain S, Hess K, Gearhart J, Geiss K, Schlager J (2005) In vitro toxicity of nanoparticles in BRL 3A rat liver cells. Toxicol in Vitro 19:975–983

Karlsson HL, Cronholm P, Gustafsson J, Moller L (2008) Copper oxide nanoparticles are highly toxic: a comparison between metal oxide nanoparticles and carbon nanotubes. Chem Res Toxicol 21:1726–1732

Ko HC, Han JS, Bächle M, Jang JH, Shin SW, Kim DJ (2007) Initial osteoblast-like cell response to pure titanium and zirconia/alumina ceramics. Dent Mater 23:1349–1355

Kosmač T, Oblak C, Jevnikar P, Funduk N, Marion L (1999) The effect of surface grinding and sandblasting on flexural strength and reliability of Y-TZP zirconia ceramic. Dent Mater 1:426–433

Krebs RA, Feder ME (1997) Deleterious consequences of Hsp70 overexpression in *Drosphila melanogaster* larvae. Cell Stress Chaperones 2:60–71

Lacefield WR (1999) Materials characteristics of uncoated/ceramic-coated implant materials. Adv Dent Res 13:21–26

Lehane M (1997) Peritrophic matrix structure and function. Annu Rev Entomol 42:525–550

Lewinski N, Colvin V, Drezek R (2008) Cytotoxicity of nanoparticles. Small 4:26–49

Li Y, Fetchko M, Lai ZC, Baker NE (2003) Scabrous and Gp150 are endosomal proteins that regulate Notch activity. Development 130:2819–2827

Liang J, Deng Z, Jiang X, Li F, Li Y (2002) Photoluminescence of tetragonal ZrO_2 nanoparticles synthesized by microwave irradiation. Inorg Chem 41:3602–3604

Lima EMCX, Koo H, Vacca Smith AM, Rosalen PL, Del Bel Cury AA (2008) Adsorption of salivary and serum proteins, and bacterial adherence on titanium and zirconia ceramic surfaces. Clin Oral Implants Res 19:780–785

Long TC, Saleh N, Tilton RD, Lowry GV, Veronesi B (2006) Titanium dioxide (P25) produces reactive oxygen species in

immortalized brain microglia (BV2): implications for nanoparticle neurotoxicity. Environ Sci Technol 40:4346–4352

Lynch I, Dawson KA (2008) Protein-nanoparticle interactions. Nano Today 3:40–47

Manicone PF, Iommetti PR, Raffaelli L (2007) An overview of zirconia ceramics: basic properties and clinical applications. J Dent 35:819–826

Martinez V, Javadi C, Ngo E, Ngo L, Lagow R, Zhang B (2007) Age-related changes in climbing behavior and neural circuit physiology in *Drosophila*. Deve Neurobiol 67:778–791

Nagy LN, Mihály J, Polyák A, Debreczeni B, Császár B, Szigyártó IC, Wacha A, Czégény Z, Jakab E, Klébert S (2015) Inherently fluorescent and porous zirconia colloids: preparation, characterization and drug adsorption studies. J Mater Chem 3:7529–7537

Nagy LN, Polyák A, Mihály J, Szécsényi Á, Szigyártó IC, Czégény Z, Jakab E, Németh P, Magda B, Szabó PT (2016) Silica@zirconia@poly (malic acid) nanoparticle: a promising nanocarrier for theranostic applications. J Mater Chem B 4: 4420–4429

Nichols CD, Becnel J, Pandey UB (2012) Methods to assay *Drosophila* behavior. JoVE (J Vis Exp) e3795

Ohlstein B, Spradling A (2006) The adult *Drosophila* posterior midgut is maintained by pluripotent stem cells. Nature 439: 470–474

Pappus, S.A., Ekka, B., Sahu, S., Sabat, D., Dash, P., Mishra, M., 2017. A toxicity assessment of hydroxyapatite nanoparticles on development and behaviour of Drosophila melanogaster. Journal of Nanoparticle Research 19: 136

Piconi C, Maccauro G (1999) Zirconia as a ceramic biomaterial. Biomaterials 20:1–25

Posgai R, Cipolla-McCulloch CB, Murphy KR, Hussain SM, Rowe JJ, Nielsen MG (2011) Differential toxicity of silver and titanium dioxide nanoparticles on *Drosophila* Melanogaster development, reproductive effort, and viability: size, coatings and antioxidants matter. Chemosphere 85: 34–42

Sabat D, Patnaik A, Ekka B, Dash P, Mishra M (2016) Investigation of titania nanoparticles on behaviour and mechanosensory organ of Drosophila melanogaster. Physiol Behav 167:76–85

Siddique YH (2012) Protective role of curcumin against the toxic effects of cyclophosphamide in the third instar larvae of transgenic *Drosophila melanogaster* (hsp70-lacZ) Bg9. Altern Med Stud 2:2–6

Sollazzo V, Palmieri A, Pezzetti F, Bignozzi CA, Argazzi R, Massari L, Brunelli G, Carinci F (2008) Genetic effect of zirconium oxide coating on osteoblast-like cells. J Biomed Mater Res 84:550–558

Song W, Onishi M, Jan LY, Jan YN (2007) Peripheral multidendritic sensory neurons are necessary for rhythmic locomotion behavior in *Drosophila* larvae. Proc Natl Acad Sci 104:5199–5204

Sotoudeh A, Jahanshahi A, Takhtfooladi MA, Bazazan A, Ganjali A, Harati MP (2013) Study on nano-structured hydroxyapatite/zirconia stabilized yttria on healing of articular cartilage defect in rabbit. Acta Bras Cir 28:340–345

Sponchia G, Ambrosi E, Rizzolio F, Hadla M, Del Tedesco A, Spena CR, Toffoli G, Riello P, Benedetti A (2015) Biocompatible tailored zirconia mesoporous nanoparticles with high surface area for theranostic applications. J Mater Chem 3:7300–7306

Takashima S, Hartenstein V (2012) Genetic control of intestinal stem cell specification and development: a comparative view. Stem Cell Rev 8:597–608

Tang S, Huang X, Chen X, Zheng N (2010) Hollow mesoporous zirconia nanocapsules for drug delivery. Adv Funct Mater 20: 2442–2447

Tsakonas A, Rand S, Matthew D, Lake JR (1999) Notch signaling: cell fate control and signal integration in development. Science 284:770–776

Wason MS, Colon J, Das S, Seal S, Turkson J, Zhao J, Baker CH (2013) Sensitization of pancreatic cancer cells to radiation by cerium oxide nanoparticle-induced ROS production. Nanomed Nanotech Biol Med 9:558–569

Wolff T, Ready DF (1991) Cell death in normal and rough eye mutants of *Drosophila*. Development 113:825–839

Yang M, Hatton-Ellis E, Simpson P (2012) The kinase Sgg modulates temporal development of macrochaetes in *Drosophila* by phosphorylation of Scute and Pannier. Development 139: 325–334

Zhang W, Yan Z, Li B, Jan LY, Jan YN (2014) Identification of motor neurons and a mechanosensitive sensory neuron in the defecation circuitry of *Drosophila* larvae. elife 3:e03293